Local control of magnetic anisotropy in transcritical permalloy thin films using ferroelectric $BaTiO_3$ domains

Sean W. Fackler,[1] Michael J. Donahue,[2] Tieren Gao,[1] Paris N. A. Nero,[1]

Sang-Wook Cheong,[3] John Cumings,[1] and Ichiro Takeuchi [1,*]

[1]*Department of Materials Science and Engineering,*

University of Maryland, College Park, Maryland 20742, USA

[2] *National Institute of Standards and Technology, Gaithersburg MD 20899, USA*

[3] *Rutgers the State University of New Jersey, Department of Physics and Astronomy,*

Piscataway, NJ 08854, USA

(Dated: October 10, 2014)

Abstract

We investigated the local coupling between dense magnetic stripe domains in transcritical permalloy (tPy) thin films and ferroelectric domains of $BaTiO_3$ single crystals in a tPy/$BaTiO_3$ heterostructure. Two distinct changes in the magnetic stripe domains of tPy were observed from the magnetic force microscopy images after cooling the heterostructure from above the ferroelectric Curie temperature of $BaTiO_3$ (120 °C) to room temperature. First, an abrupt break in the magnetic stripe domain direction was found at the ferroelectric a-c-domain boundaries due to an induced change in in-plane magnetic anisotropy. Second, the magnetic stripe domain period increased when coupled to a ferroelectric a-domain due to a change in out-of-plane magnetic anisotropy. Micromagnetic simulations reveal that local magnetic anisotropy energy from inverse magnetostriction is conserved between in-plane and out-of-plane components.

The strain controlled magnetic properties of thin films is widely investigated for future applications in random access memories[1,2], sensors[3] and transducers[4]. Such devices for controlling magnetic domains and magnetization direction are typically made of magnetostrictive films in intimate contact with ferroelectric materials. The effect of electric-field induced strains on these devices is usually studied by monitoring changes in macroscopic properties such as magnetic hysteresis loops[5–8]. There are, however, only a handful of studies investigating the local microscopic interactions of ferroelectric and ferromagnetic domains[9–14]. Local coupling of ferroelectric and ferromagnetic domains has been observed with polarized microscopy for 30 nm CoFe on $BaTiO_3$ with applied electric fields[9,10], with scanning probe microscopy of an all-thin-film Ni/PZT device[11], and using scanning electron microscopy with polarization analysis[15].

In this study we used magnetic force microscopy (MFM) to image the magnetic domain pattern of transcritical permalloy (tPy) films[16–18] deposited on $BaTiO_3$ single crystals. They are called transcritical because magnetic stripe domains (MSDs) form only above a critical thickness. Since the 1960's tPy has been studied because of its dense MSDs which are sensitive to strain[19], thickness[20], and magnetic anisotropy energy[18,21]. The MSDs arise from a weak out-of-plane magnetic anisotropy[16–18,20,22,23] and they can be clearly imaged by MFM.

We experimentally observe local changes in the magnetic anisotropy of tPy consistent with the ferroelectric a-c-domain pattern of a $BaTiO_3$ crystal after cooling from above the Curie temperature (T_C) of $BaTiO_3$. MFM images of the magnetic domain patterns give us quantitative information about average in-plane magnetization direction and out-of-plane anisotropy energies. Micromagnetic simulations of the MSD orientation and the periodicity show that inverse magnetostriction from a uniaxial tensile strain on the tPy over ferroelectric a-domains can account for the observed changes.

A 115 nm thick permalloy film was sputtered on a 200 μm thick and 3 mm wide $BaTiO_3$ butterfly single-crystal[24] at room temperature. The deposition pressure was 1.6 Pa (12 mTorr) and the deposition rate was 15 nm/min. Wavelength dispersive spectroscopy confirmed the permalloy film composition as 81 at% nickel. The transcritical thickness was determined by keeping all other sputtering conditions the same and varying only the film thickness. MFM and vibrating sample magnetometer measurements were taken to confirm the presence or absence of MSDs and the unique magnetic hysteresis loop associated with the MSDs,

respectively. This gave the transcritical thickness for our sputtering conditions as (115 ± 20) nm. During the film optimization process we verified that the stripe domain period (Λ) had the expected square root dependence on the tPy film thickness[16,18,22] as shown in Fig. 1(a).

The MSD period and orientation were determined by atomic force microscope (AFM) calibrated with a 3 μm grid. Two dimensional Fast Fourier Transform (2D-FFT) analysis of MFM images was used to obtain accurate stripe domain information. The thermal treatment was done in air by placing the heterostructure on a hotplate and immediately after reaching 150 °C was set on a metal block to cool to room temperature. The ferroelectric domains of the $BaTiO_3$ single crystal were imaged by piezo-response force microscopy (PFM). Two separate simulations using the object oriented micromagnetic framework (OOMMF)[25] software were carried out.

The PFM image in Fig. 1(b) shows a typical ferroelectric a-domain of about 5 μm width for a $BaTiO_3$ single-crystal prior to tPy deposition. The a-domains are long in the crystallographic (100) direction and the ferroelectric c-domains are wider[26]. The strain direction for a-domains lies perpendicular to the length of the a-domain[27,28], or the (010) direction in Fig. 1(b). The ferroelectric c-domains are strained out-of-plane in the (001) direction hence presenting a cubic face of the tetragonal unit cell to the surface. A corresponding modulation in strain is present at the surface of the $BaTiO_3$ crystal from the ferroelectric a-c-domain pattern[29]. More specifically, there is an isotropic strain over c-domains and a uniaxial tensile strain over a-domains of 1.1%. The locations of ferroelectric domain boundaries in $BaTiO_3$ after tPy deposition were deduced from the $BaTiO_3$ surface topography. The $BaTiO_3$ surface topography arises from the tetragonal lattice distortion which causes height displacement at the surface in order to lattice match the differently oriented ferroelectric domains. This effect was confirmed with AFM/PFM images (not shown) and agrees with previous studies[26].

A tPy film was deposited after the ferroelectric a-c-domains of $BaTiO_3$ were verified with PFM. Fig. 1(c) shows a cross-sectional scanning electron microscope (SEM) micrograph of the tPy/$BaTiO_3$ heterostructure. The columnar microstructure in the tPy can be clearly seen. The competition between shape anisotropy, out-of-plane magnetic anisotropy, magnetostatic, and magnetic exchange energies in the tPy results in the alternating up and down magnetic moments giving the strong contrast in MFM images[30].

There is, however, still a large in-plane component to the magnetization taken as the direction of the stripe domain lines. Fig. 1(d) shows the in-plane magnetic hysteresis loop of tPy where at low fields a sharp switching occurs and at higher fields a linear slope is present until saturation. The remnant value of the in-plane hysteresis loop indicates that there is still a large in-plane component of the magnetization lying along the direction of the stripes despite the alternating out-of-plane magnetization components[16,30–32].

Dozens of areas were imaged with MFM before and after cooling the tPy/$BaTiO_3$ heterostructure from above the T_C of $BaTiO_3$ to room temperature. Before thermal treatment, stripe domains were found covering the sample and often pointed in a single direction irrespective of the underlying ferroelectric $BaTiO_3$ domains (as shown in Fig. 2(a)). This indicates that the magnetic anisotropy of the as-deposited tPy was not affected by the underlying ferroelectric substrate before thermal treatment. The initial stripe domain direction shown in Fig. 2(a) is an arbitrary angle since no deliberate magnetic fields were applied during the deposition.

Fig. 2(b) shows the MFM image after cooling from above $BaTiO_3$'s T_C back to room temperature. The striking result is the sharp break of stripe domain orientation at the ferroelectric domain boundaries observed only after thermal treatment. The ferroelectric domain boundaries depicted in Fig. 2 are deduced from the simultaneously captured AFM images (not shown). One clearly sees that stripe domain orientation changes only over the ferroelectric a-domain area and remains in the same direction over c-domains.

As a comparison, we also investigated the strain effect of Si on the magnetic domains of tPy in a tPy/Si sample which was made with the same conditions as tPy/$BaTiO_3$. No changes were observed in the MSD configuration comparing the MFM images before and after thermal treatment for the tPy/Si sample. This is due to the fact that Si does not have strain modulation over its surface. Therefore, the change of MFM images in the tPy/$BaTiO_3$ before and after thermal treatment is from the uniaxial strain of $BaTiO_3$'s ferroelectric a-domains.

We also consider the strain contribution from thermal expansion for the control sample. Silicon's thermal expansion coefficient[33] is $\alpha_{Si} = 2.56 \times 10^{-6}\,C^{-1}$ while that for permalloy[34] is $\alpha_{Ni_{80}Fe_{20}} = 11.5 \times 10^{-6}\,C^{-1}$. For a temperature change during thermal treatment of ΔT = 130 °C from room temperature (20 °C) to the 150 °C we get a thermal strain of $\Delta T \times (\alpha_{Ni_{80}Fe_{20}} - \alpha_{Si}) = \varepsilon_{Ni_{80}Fe_{20}} - \varepsilon_{Si} = 0.1\%$. This strain from thermal

expansion is an order of magnitude smaller than that provided by the tetragonal distortion of the $BaTiO_3$. In addition, the strain from thermal expansion is isotropic in comparison to $BaTiO_3$'s uniaxial strain from tetragonal distortion.

Changes of the stripe domain orientation are due to the inverse magnetostrictive effect of tPy. Permalloy at the $Ni_{81}Fe_{19}$ composition is slightly negative magnetostrictive. Applying tensile strain to a negative magnetostrictive material forces the magnetic moments to point perpendicular to the direction of tensile strain[35]. Fig. 2(b) shows that stripe domains were forced to point almost perpendicular to the uniaxial tensile strain or along the a-domain length. The competition of in-plane magnetostatic, magnetoelastic, and exchange energy in the tPy prevents a full alignment of the stripe domains along the a-domain length. On the other hand, stripe domains over ferroelectric c-domains do not change after the thermal treatment because the strain over c-domains is always isotropic. $BaTiO_3$ is cubic above T_C[36] and below T_C, the cubic side of the unit cell faces the surface for ferroelectric c-domains.

Micromagnetic simulations of the stripe domain pattern were carried out to confirm that the local magnetic anisotropy of tPy can be controlled by strain from $BaTiO_3$'s ferroelectric domains. The first simulation is of the sharp breaks in MSD orientation in Fig. 2(b). Based on previous work for tPy[16,18,30], we take the direction parallel to the stripe domain lines in the MFM images to be the direction of the average in-plane magnetization. We set the in-plane magnetic anisotropy energy of the simulated tPy as K^{IP} = 3 kPa which is close to other cited values[37]. In the c-domain areas we chose a magnetic anisotropy direction the same as the stripes in Fig. 2(a) before thermal treatment. The magnetic anisotropy over the ferroelectric a-domain area points along the domain length as deduced from the phenomenology of inverse magnetostriction described above. Using the same crystallographic axes and domain configuration as Fig. 1(b) we input an initial magnetization direction of $(1\bar{1}0)$ to OOMMF. The simulation dimensions were 4096 nm × 4096 nm × 8 nm with a cell size of 8 nm. Edge effects were reduced by doing an edge-field computation[38] for each of the four edges in the x-y plane and any edge effects were cropped from the figure.

The bottom of Fig. 2(b) shows the results of the in-plane simulation where the direction of magnetization from OOMMF agrees with the stripe domain direction in experimental MFM data above. The in-plane magnetic anisotropy magnitude was used to match simulated and experimental magnetization directions over the ferroelectric a-c-domain pattern. If K^{IP} is too

small the moments over the a-domain turn towards those of the c-domains. If K^{IP} is too large then moments over the a-domain point directly along the a-domain length in contradiction with experiment. Now we use the equation for inverse magnetostriction to show that this magnetic anisotropy energy originates from strain. The magnetic anisotropy energy $K^{IP} = -\frac{3}{2}\lambda\,\sigma$ where λ is the magnetostriction constant and the stress is $\sigma = Y\varepsilon/1 - v^2$. Constants used for tPy were Young's modulus[39,40] $Y = 190 \pm 13$ GPa, Poisson's ratio $v = 0.37$ and strain from the $BaTiO_3$ substrate was $\varepsilon = 1.1 \pm 0.1\%$. We solved for the magnetostriction constant of tPy as $\lambda_{IP} = (-0.8 \pm 0.1)$ μm/m. This calculated magnetostriction value agrees with recent studies[35] and is convincing evidence that the magnetic anisotropy energy is from the elastic coupling of the tPy to the ferroelectric $BaTiO_3$ substrate.

We also observed a modulation of stripe domain period, or stripe domain width, over the ferroelectric a-c-domain pattern after the multiferroic heterostructure was cooled from above the T_C of $BaTiO_3$. Figs. 3(a) and 3(b) show that stripe domain period changed systematically over different ferroelectric domains. Fig. 3(b) shows that stripe domains over ferroelectric a-domains have a larger period than over c-domains. 2D-FFT analysis[41] taken over the whole image gave the MSD period over ferroelectric a-domains as Λ_a = (233 ± 1) nm and MSD period over ferroelectric c-domains as Λ_c = (226 ± 1) nm. The error in period is calculated as the total image width (20 μm) divided by the number of pixels (512 pixels) divided by the number of stripes averaged over (30 stripes) and rounded. Pant et al.[21] has pointed out that stripe domain period should increase as out-of-plane anisotropy energy is lowered. This trend was also suggested by Murayama et al., from his description of critical thickness[18]. Based on this we expect the stripe domains with larger period to have less out-of-plane magnetic anisotropy energy.

To confirm this strain-based control of out-of-plane magnetic anisotropy we carried out a second simulation on the change observed in the MSD period. We used one-dimensional periodic boundary conditions parallel with the stripe domain line direction to reduce computational expense. Fig. 3(c) shows a cartoon of the second simulation where simulated in-plane and out-of-plane magnetic moments can be visualized as black arrows and as color. The simulated stripe period is from the z-component of the magnetization averaged through the thickness of the film. The full simulation is a cross-section of the stripe domains of dimensions 8192 nm × 64 nm (periodic) × 114 nm with a cell size of 2 nm. An out-of-plane

anisotropy energy for the ferroelectric a-domain of $K_a^{OOP} = 27$ kPa gave a calculated stripe domain period of $\Lambda_a^{sim} = 233.9$ nm. A larger out-of-plane anisotropy energy over ferroelectric c-domains of $K_c^{OOP} = 30$ kPa gave $\Lambda_c^{sim} = 227.5$ nm. Some boundary effects in the cross section were evident and were not included in the calculated stripe period. The calculated stripe domain periods agree with their experimental counterparts assuming the trend of stripe domain period with out-of-plane anisotropy energy suggested earlier by Pant et al. Notice that $K_c^{OOP} - K_a^{OOP} = 3$ kPa is the same energy for the change of stripe domain orientation in-plane. The reduction of the out-of-plane anisotropy energy over the ferroelectric a-domain is the same as the energy it takes to change the stripe domain orientation in-plane. We propose that the thin-film geometry causes a preference for the magnetic anisotropy to turn in-plane instead of the less energetically favorable out-of-plane direction.

In conclusion, we experimentally observed the modification of magnetic stripe domain orientation and period in tPy after cooling the tPy/$BaTiO_3$ (001) heterostructure from above the T_C of $BaTiO_3$ to room temperature. MFM investigation shows that the stripe domains sharply changed orientation at the ferroelectric domain boundary and the stripe domain period is larger over the ferroelectric a-domains compared to stripe domains over ferroelectric c-domains. OOMMF simulations indicate that a 3kPa in-plane magnetic anisotropy energy accounts for the change in the magnetic stripe domain orientation over the ferroelectric a-domain and that an equal decrease in the out-of-plane anisotropy energy accounts for the increase of the stripe period over the ferroelectric a-domain. This nanoscale control of magnetic anisotropy energy arises from the 1% strain of the $BaTiO_3$ substrate on the magnetostrictive tPy film. Future studies will include the effects of an electric field on similar heterostructures. With the demonstration of strain-mediated control of magnetic anisotropy and our previous result of local control of ferroelectric domains[42], we are one step closer to making compact and efficient memory devices.

* Electronic address: takeuchi@umd.edu

We acknowledge the support of the Maryland NanoCenter and its NispLab. This work has been supported by the UMD-NSF-MRSEC under grant DMR 05-20471.

[1] K. Roy, S. Bandyopadhyay, and J. Atulasimha, Appl. Phys. Lett. **99**, 063108 (2011).

[2] J.-M. Hu, Z. Li, J. Wang, and C.W. Nan, J. Appl. Phys. **107**, 093912 (2010).

[3] C. Israel, N.D. Mathur, and J.F. Scott, Nat. Mater. **7**, 93 (2008).

[4] J. Ma, J. Hu, Z. Li, and C.-W. Nan, Adv. Mater. **23**, 1062 (2011).

[5] Y. Zhang, J. Liu, X.H. Xiao, T.C. Peng, C.Z. Jiang, Y.H. Lin, and C.W. Nan, J. Phys. Appl. Phys. **43**, 082002 (2010).

[6] T. Nan, Z. Zhou, M. Liu, X. Yang, Y. Gao, B.A. Assaf, H. Lin, S. Velu, X. Wang, H. Luo, J. Chen, S. Akhtar, E. Hu, R. Rajiv, K. Krishnan, S. Sreedhar, D. Heiman, B.M. Howe, G.J. Brown, and N.X. Sun, Sci. Rep. **4**, (2014).

[7] S. Geprägs, A. Brandlmaier, M. Opel, R. Gross, and S.T.B. Goennenwein, Appl. Phys. Lett. **96**, 142509 (2010).

[8] A. Brandlmaier, S. Geprägs, G. Woltersdorf, R. Gross, and S.T.B. Goennenwein, J. Appl. Phys. **110**, 043913 (2011).

[9] T.H.E. Lahtinen, J.O. Tuomi, and S. van Dijken, IEEE Trans. Magn. **47**, 3768 (2011).

[10] T.H.E. Lahtinen, K.J.A. Franke, and S. van Dijken, Sci. Rep. **2**, (2012).

[11] T.-K. Chung, G.P. Carman, and K.P. Mohanchandra, Appl. Phys. Lett. **92**, 112509 (2008).

[12] Y.-H. Chu, L.W. Martin, M.B. Holcomb, M. Gajek, S.-J. Han, Q. He, N. Balke, C.-H. Yang, D. Lee, W. Hu, Q. Zhan, P.-L. Yang, A. Fraile-Rodríguez, A. Scholl, S.X. Wang, and R. Ramesh, Nat. Mater. **7**, 478 (2008).

[13] J.T. Heron, M. Trassin, K. Ashraf, M. Gajek, Q. He, S.Y. Yang, D.E. Nikonov, Y.-H. Chu, S. Salahuddin, and R. Ramesh, Phys. Rev. Lett. **107**, 217202 (2011).

[14] T. Brintlinger, S.-H. Lim, K.H. Baloch, P. Alexander, Y. Qi, J. Barry, J. Melngailis, L. Salamanca-Riba, I. Takeuchi, and J. Cumings, Nano Lett. **10**, 1219 (2010).

[15] J. Unguris, S.R. Bowden, D.T. Pierce, M. Trassin, R. Ramesh, S.-W. Cheong, S. Fackler, and I. Takeuchi, APL Mater. **2**, 076109 (2014).

[16] N. Saito, H. Fujiwara, and Y. Sugita, J. Phys. Soc. Jpn. **19**, 1116 (1964).

[17] R.J. Spain, Appl. Phys. Lett. **6**, 8 (1965).

[18] Y. Murayama, J. Phys. Soc. Jpn. **21**, 2253 (1966).

[19] W. Karboul-Trojet, D. Faurie, E. Aït-Yahiatène, Y. Roussigné, F. Mazaleyrat, and S.M. Chérif, J. Appl. Phys. **111**, 07A926 (2012).

[20] J. Ben Youssef, N. Vukadinovic, D. Billet, and M. Labrune, Phys. Rev. B **69**, 174402 (2004).

[21] B.B. Pant and K. Matsuyama, Jpn. J. Appl. Phys. **32**, 3817 (1993).

[22] N. Amos, R. Fernandez, R. Ikkawi, B. Lee, A. Lavrenov, A. Krichevsky, D. Litvinov, and S. Khizroev, J. Appl. Phys. **103**, 07E732 (2008).

[23] A.V. Svalov, I.R. Aseguinolaza, A. Garcia-Arribas, I. Orue, J.M. Barandiaran, J. Alonso, M.L. FernAndez-Gubieda, and G.V. Kurlyandskaya, IEEE Trans. Magn. **46**, 333 (2010).

[24] J.P. Remeika and W.M. Jackson, J. Am. Chem. Soc. **76**, 940 (1954).

[25] Donahue, M.J. and Porter, D.G., *OOMMF User's Guide, Version 1.0* (National Institute of Standards and Technology, Gaithersburg, MD, 1999).

[26] M. Takashige, S.-I. Hamazaki, N. Fukurai, and F. Shimizu, J. Phys. Soc. Jpn. **66**, 1848 (1997).

[27] N.T. Tsou, P.R. Potnis, and J.E. Huber, Phys. Rev. B **83**, 184120 (2011).

[28] S.V. Kalinin, B.J. Rodriguez, S. Jesse, J. Shin, A.P. Baddorf, P. Gupta, H. Jain, D.B. Williams, and A. Gruverman, Microsc. Microanal. **12**, 206 (2006).

[29] J.-H. Park, J.-H. Park, K.-B. Lee, T.-Y. Koo, H.S. Youn, Y.-D. Ko, J.-S. Chung, J.Y. Hwang, and S.-Y. Jeong, Appl. Phys. Lett. **91**, 012906 (2007).

[30] A. Hubert and R. Schäfer, *Magnetic Domains: The Analysis of Magnetic Microstructures*, Corrected edition (Springer, 2008).

[31] L.M. Alvarez-Prado, G.T. Pérez, R. Morales, F.H. Salas, and J.M. Alameda, Phys. Rev. B **56**, 3306 (1997).

[32] D. Clarke, O.A. Tretiakov, and O. Tchernyshyov, Phys. Rev. B **75**, 174433 (2007).

[33] P. Becker, P. Scyfried, and H. Siegert, Z. Für Phys. B Condens. Matter **48**, 17 (1982).

[34] E.A. Owen, E.L. Yates, and A.H. Sully, Proc. Phys. Soc. **49**, 323 (1937).

[35] C.B. Hill, W.R. Hendren, R.M. Bowman, P.K. McGeehin, M.A. Gubbins, and V.A. Venugopal, Meas. Sci. Technol. **24**, 045601 (2013).

[36] R. Clarke, J. Appl. Crystallogr. **9**, 335 (1976).

[37] M. Takahashi, D. Watanabe, T. Kōno, and S. Ogawa, J. Phys. Soc. Jpn. **15**, 1351 (1960).

[38] R.D. McMichael and M.J. Donahue, IEEE Trans. Magn. **33**, 4167 (1997).

[39] M.M. Yang and J.A. Aboaf, J. Appl. Phys. **66**, 3734 (1989).

[40] H. Deng, M.K. Minor, and J.A. Barnard, IEEE Trans. Magn. **32**, 3702 (1996).

[41] D. Nečas and P. Klapetek, Cent. Eur. J. Phys. **10**, 181 (2012).

[42] V. Anbusathaiah, D. Kan, F.C. Kartawidjaja, R. Mahjoub, M.A. Arredondo, S. Wicks, I. Takeuchi, J. Wang, and V. Nagarajan, Adv. Mater. **21**, 3497 (2009).

FIGURE CAPTIONS

FIG. 1. (a) Thickness dependence of stripe domain period (Λ) on log scale. (b) Typical PFM image of the $BaTiO_3$ single-crystal with ferroelectric a-c-domains labelled. (c) SEM cross-section of our tPy/$BaTiO_3$ heterostructure showing the microstructure of the tPy. (d) Normalized in-plane magnetic hysteresis loop of tPy.

FIG. 2. MFM images of the tPy/$BaTiO_3$ heterostructure before thermal treatment (a) and after thermal treatment (b). Ferroelectric domain boundaries are indicated by translucent yellow lines. White arrows indicate average stripe domain orientation. The double-sided arrow in (b) points along the uniaxial strain direction over the a-domain. Ferroelectric a-c-domains are labelled in white. Results of in-plane OOMMF simulation are pictured below experimental MFM results in (b).

FIG. 3(a) White boxes surround representative areas of the MFM image for 2D-FFT analysis. The transforms below each respective area have radial lines where cross-sections were taken. The bar is 10 μm^{-1}. (b) Cross-sections of each transform were overlaid, color-coded, and plotted versus stripe domain period. (c) Cartoon of out-of-plane OOMMF simulation showing the stripe domain period, Λ, direction of the out-of-plane anisotropy energy K^{OOP} and direction of the periodic boundary conditions. Black arrows are simulated magnetic moments in their respective planes and the color wheel indicates the magnetic moment direction on each plane.

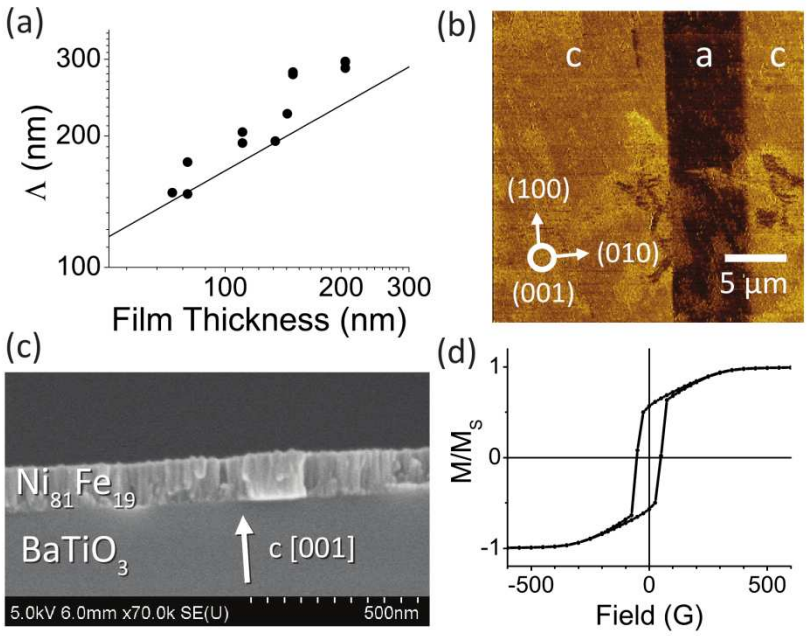

FIG. 1. (a) Thickness dependence of stripe domain period (Λ) on log scale. (b) Typical PFM image of the $BaTiO_3$ single-crystal with ferroelectric a-c-domains labelled. (c) SEM cross-section of our tPy/$BaTiO_3$ heterostructure showing the microstructure of the tPy. (d) Normalized in-plane magnetic hysteresis loop of tPy.

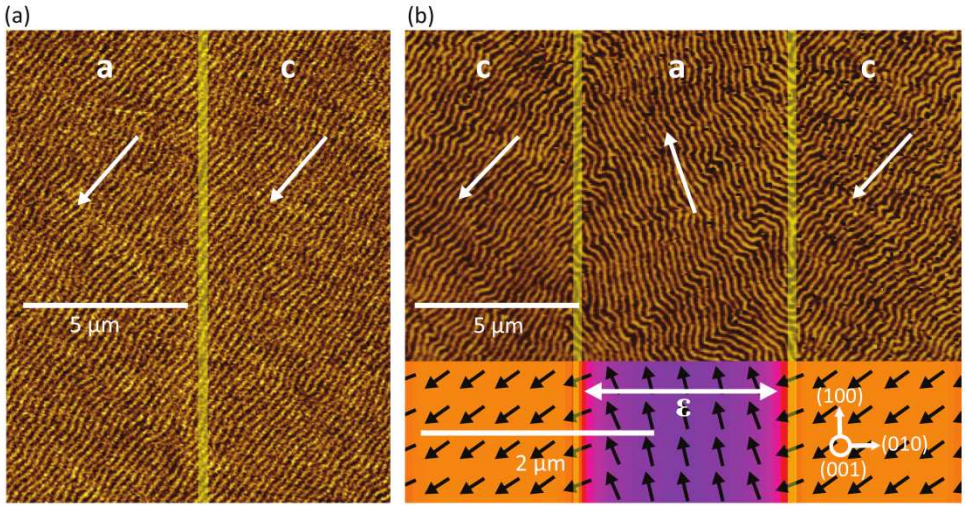

FIG. 2. MFM images of the tPy/$BaTiO_3$ heterostructure before thermal treatment (a) and after thermal treatment (b). Ferroelectric domain boundaries are indicated by translucent yellow lines. White arrows indicate average stripe domain orientation. The double-sided arrow in (b) points along the uniaxial strain direction over the a-domain. Ferroelectric a-c-domains are labelled in white. Results of in-plane OOMMF simulation are pictured below experimental MFM results in (b).

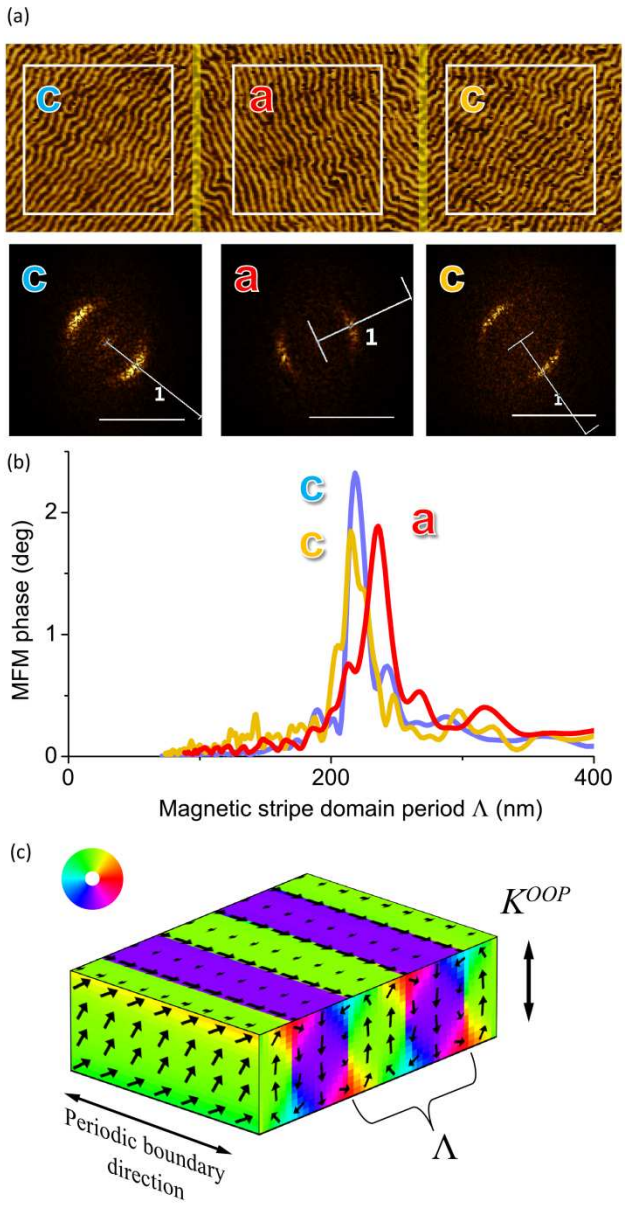

FIG. 3(a) White boxes surround representative areas of the MFM image for 2D-FFT analysis. The transforms below each respective area have radial lines where cross-sections were taken. The bar is 10 μm^{-1}. (b) Cross-sections of each transform were overlaid, color-coded, and plotted versus stripe domain period. (c) Cartoon of out-of-plane OOMMF simulation showing the stripe domain period, Λ, direction of the out-of-plane anisotropy energy K^{OOP} and direction of the periodic boundary conditions. Black arrows are simulated magnetic moments in their respective planes and the color wheel indicates the magnetic moment direction on each plane.